JMEPEG (2019) 28:2562–2572
https://doi.org/10.1007/s11665-019-04058-3

1059-9495/$19.00

Effect of $MgCl_2$ on the Corrosion Behavior of Copper Under Periodic Wet/Dry Cycle Condition

Chen Pan, Mingxiao Guo, and Zhenyao Wang

(Submitted March 20, 2018; in revised form March 28, 2019; published online April 29, 2019)

The corrosion behaviors of copper under periodic wet/dry cycle conditions were investigated. The characteristics of the corrosion product formed on copper were analyzed by x-ray diffraction, scanning electron microscopy, energy-dispersive spectroscopy, and in situ electrochemical impedance spectroscopy. Weight loss results showed that the corrosion of copper under an $MgCl_2$ deposition condition was more severe than that under NaCl. The main corrosion products formed on the tested sample under NaCl deposition condition consisted of $Cu_2Cl(OH)_3$ and Cu_2O, while those under the $MgCl_2$ deposition condition consisted of $Cu_2Cl(OH)_3$ and $Mg_2(OH)_3Cl{\cdot}4H_2O$. In the case of the NaCl deposition condition, a two-layered structure formed during the corrosion process. However, the corrosion product layer formed on copper under the $MgCl_2$ deposition condition had an extremely loose structure. The effect of $MgCl_2$ on the corrosion mechanism of copper is discussed.

Keywords atmospheric corrosion, copper, in situ electrochemical impedance spectroscopy, $MgCl_2$

1. Introduction

The atmospheric corrosion of metals is attributed to chemical and electrochemical reactions between the materials affected by environmental factors including temperature, relative humidity (RH), and corrosive medium. In other words, it occurs owing to the interactions of the materials with climatic factors. Many studies have been carried out to investigate the corrosion behaviors and mechanisms of metals subjected to various atmospheric environments such as rural, industrial, and coastal atmospheres, which are characterized by different environmental factors (Ref 1-3). In recent years, the rich mineral resources in salt lakes have attracted increasing attention. For example, up to 70% of the world lithium reserves, which are crucial for the development of lithium batteries, are contained in salt lakes (Ref 4). However, the salt lake atmosphere is extremely dry and usually rich in $MgCl_2$, very different from other typical atmospheres. This implies that metals exposed to a salt lake atmosphere would have distinct corrosion behaviors (Ref 5-8). Li et al. reported that Cl^- has a significant influence on the corrosion of a weathering steel under a salt lake atmosphere (Ref 5). Wang et al. revealed that the large amount of Mg in the rust layer had a large influence on the corrosion behavior of a weathering steel subjected to an indoor wet/dry cyclic test (Ref 6). Wang et al. (Ref 7) also investigated the corrosion behavior of a carbon steel exposed to a natural salt lake atmosphere. The experimental results indicated that Mg gradually accumulated in the rust layer formed on the carbon steel surface by replacing some ferric ions in the intermediates to form the corrosion product $Mg_4Fe(OH)_8OCl{\cdot}xH_2O$. This corrosion product provided anion selectivity of the rust layer, promoted the diffusion of chloride ions, destroyed the structure of the rust layer, and finally accelerated the corrosion of the carbon steel. Wang et al. (Ref 8) reported that the corrosion rate of AA2024-T3 exposed to a salt lake atmosphere was higher than those for coastal and industrial atmospheres. In addition, $[Mg_{1-x}Al_x(OH)_2]^{x^+}Cl_x^- \cdot mH_2O$ was observed in the corrosion products, which demonstrates that Mg^{2+} was involved in the corrosion process as a reactant.

Northwest China has hundreds of salt lakes as well as arid-rainless and land salinization characteristics, which make the climatic conditions different from those of the central and eastern regions. With the gradual implementation of the western development strategy and rapid development of the local economy, more communication and power facilities will be needed in the western region. Copper is of significance in communication and electronics industries owing to its high conductivity. It is thus essential to investigate the corrosion behavior and mechanism of copper exposed to a salt lake atmosphere. Although many studies have been carried out to investigate the atmospheric corrosions of copper and its alloys through various typical outdoor exposures (Ref 9-11) and laboratory tests (Ref 12-14), no extensive studies have been performed on the corrosion behavior of copper subjected to a salt lake atmosphere.

The aim of this study was to investigate the corrosion behavior and mechanism of copper exposed to a simulated salt lake atmosphere using a weight loss measurement, scanning electron microscopy (SEM), x-ray diffraction (XRD), and in situ electrochemical impedance spectroscopy (EIS). The results of this study provide a detailed understanding of the corrosion behavior of copper under a natural salt lake atmosphere.

2. Experimental Methods

2.1 Material Preparation

High-purity copper ($>$ 99.99 wt.%) was selected as the test material. The samples for loss gain and weight loss measure-

Chen Pan, Mingxiao Guo, and **Zhenyao Wang**, Environmental Corrosion Center, Institute of Metal Research, Chinese Academy of Science, Shenyang 110016, China. Contact e-mails: cpan@imr.ac.cn and zhywang@imr.ac.cn.

ments were cut to dimensions of 50 × 25 × 2 mm^3 and were ultrasonically cleaned in acetone, dried, weighed, and stored in a moisture-free environment. The samples for the electrochemical test were cut to dimensions of the size of 10 × 10 × 2 mm^3 and were then embedded in epoxy resin, leaving an exposed working area of 1 cm^2. The electrochemical test samples were ground with a 2000-grit SiC paper and then degreased by acetone, dehydrated with ethanol, and finally dried for 24 h.

2.2 Electrode Preparation

A two-electrode system with a comb-like arrangement was used for the in situ EIS measurements. In order to utilize the collection of electrical signal, comb-like electrodes separated by a microscale distance were prepared from pure copper plates with dimensions of 10 × 10 × 2 mm^3. The plates were separated from each other by a thin insulator and then embedded in epoxy. A schematic of the electrode design is presented in Ref 15, which shows that the distance between the two plates is approximately 60 μm. After grinding with the SiC paper to 2000 grit, the electrodes separated by the microscale distance were stored in a desiccator for 24 h and then subjected to the wet/dry cyclic corrosion tests.

2.3 Wet/Dry Cyclic Accelerated Test

$MgCl_2$ and NaCl are the most common corrosive media in salt lake and marine atmospheres. In order to distinguish the corrosion mechanisms of copper under $MgCl_2$ and NaCl deposition conditions and to elucidate the role of magnesium ions, a comparative group experiment was performed using a NaCl corrosive medium. The wet/dry cycling test was carried out using a Weiss–Voetsch temperature and climatic test system. The corrosion tests involved the following steps within a period of 24 h: (1) coating of the sample surface with 20 μL/cm^2 of 0.1 mol/L $MgCl_2$ (simulating a salt lake atmosphere) or 0.2 mol/L NaCl (comparative group experiment), (2) drying of the sample in an oven at 40 °C, (3) wetting of the sample in the test box set at 30 °C and RH of 80% for 60 min, (4) drying of the sample again in the test box maintained at 30 °C and RH of 20% for 120 min, and (5) steps (3) and (4) are repeated seven times. The test samples were retrieved for analysis after 96, 192, 288, 384, and 480 h. For gravimetric experiments, the corrosion products on the retrieved samples were chemically removed by soaking in a specific solution (100 mL H_2SO_4 + 900 mL distilled water) at 20–25 °C according to the International Organization for Standardization (ISO) 8407 standard (Ref 16).

2.4 Electrochemical Measurements

As an effective method for investigation of the corrosion behaviors of metals, EIS is usually employed to nondestructively estimate the corrosion rate and to determine the corrosion mechanisms related to the interfacial processes (Ref 17). Particularly, the in situ EIS technique can provide instantaneous information on the prevailing electrochemical processes, which are essential for studies on the corrosion mechanisms of metals (Ref 18-20). The in situ EIS measurements were performed using a PARSTAT 2273 potentiostat/galvanostat. The EIS data of the electrodes (separated by the microscale distance) with $MgCl_2$ and NaCl particles were measured in the corrosion test box at an RH of 80%. The amplitude of the AC voltage was 10 mV, while the frequency range was in the range of 10^5 to 10^{-2} Hz. The frequency sweep in EIS is always performed from high to low values.

2.5 Characterization of Corrosion Products

The surface and cross-sectional morphologies of the corrosion products were observed by SEM and energy-dispersive spectrometer (SEM/EDS, XL30FEG). The samples used in the observation of the cross-sectional morphologies were embedded in epoxy resin. An XRD analysis was used to characterize the crystalline corrosion products formed on copper. The XRD measurements were performed using a Rigaku D/max 2000 diffractometer with a Cu K_α target at 50 kV, 250 mA, 2θ of 10–80°, and scanning speed of 2° min^{-1}. The wavelength of the Cu K_α radiation is 1.54056 Å.

3. Results

3.1 Mass Loss of Copper

The extent of corrosion can be determined by measuring the mass loss of copper before and after the test. The mass loss measurement results showed that the mass loss of copper under the $MgCl_2$ deposition condition after 480 h of exposure is 27.0 ± 2.3 g/m^2, while that under NaCl is 20.4 ± 0.4 g/m^2. Therefore, the mass loss of copper under the $MgCl_2$ deposition condition is higher than that under NaCl, which demonstrates that the corrosion of copper in the case of the $MgCl_2$ deposition condition is more severe. Under the same concentration of chloride ions, it can be deduced that the Mg elements may accelerate the corrosion of copper.

3.2 Electrochemical Measurements

In order to provide further insights, we employed an in situ EIS analysis to explain the structure and protective role of the corrosion products formed on the surface using the electrodes separated by the microscale distance, as in the previous study (Ref 15). Figure 1 shows Nyquist and Bode plots of copper as a function of the corrosion time under both deposition conditions. In the case of copper under the $MgCl_2$ deposition condition, the low-frequency impedance exhibits a tail corresponding to the Warburg impedance during the whole corrosion process (Fig. 1a). The existence of Warburg impedance indicates the diffusion-controlled corrosion process on the sample surface (Ref 21), including the cathodic diffusion of dissolved oxygen from the solution to the surface and anodic diffusion of soluble copper species in the opposite direction (Ref 22). However, for the copper under the NaCl deposition condition, the Warburg impedance can be measured only in the initial corrosion stage (Fig. 1a). With the progress of the corrosion, the Warburg impedance disappeared, followed by irregular changes in the impedance spectra. The changes in magnitude and shape of the impedance spectra with the progress of the corrosion indicate that the structure of the corrosion product layer also changed. In addition, the Bode plots in Fig. 1(b) show three time constants during the whole corrosion process for the copper under the $MgCl_2$ deposition condition. However, under the NaCl deposition condition, three time constants were obtained at the initial stages, while two at the later stages, after the corrosion substantially progressed (Fig. 1d). According to the Bode plots,

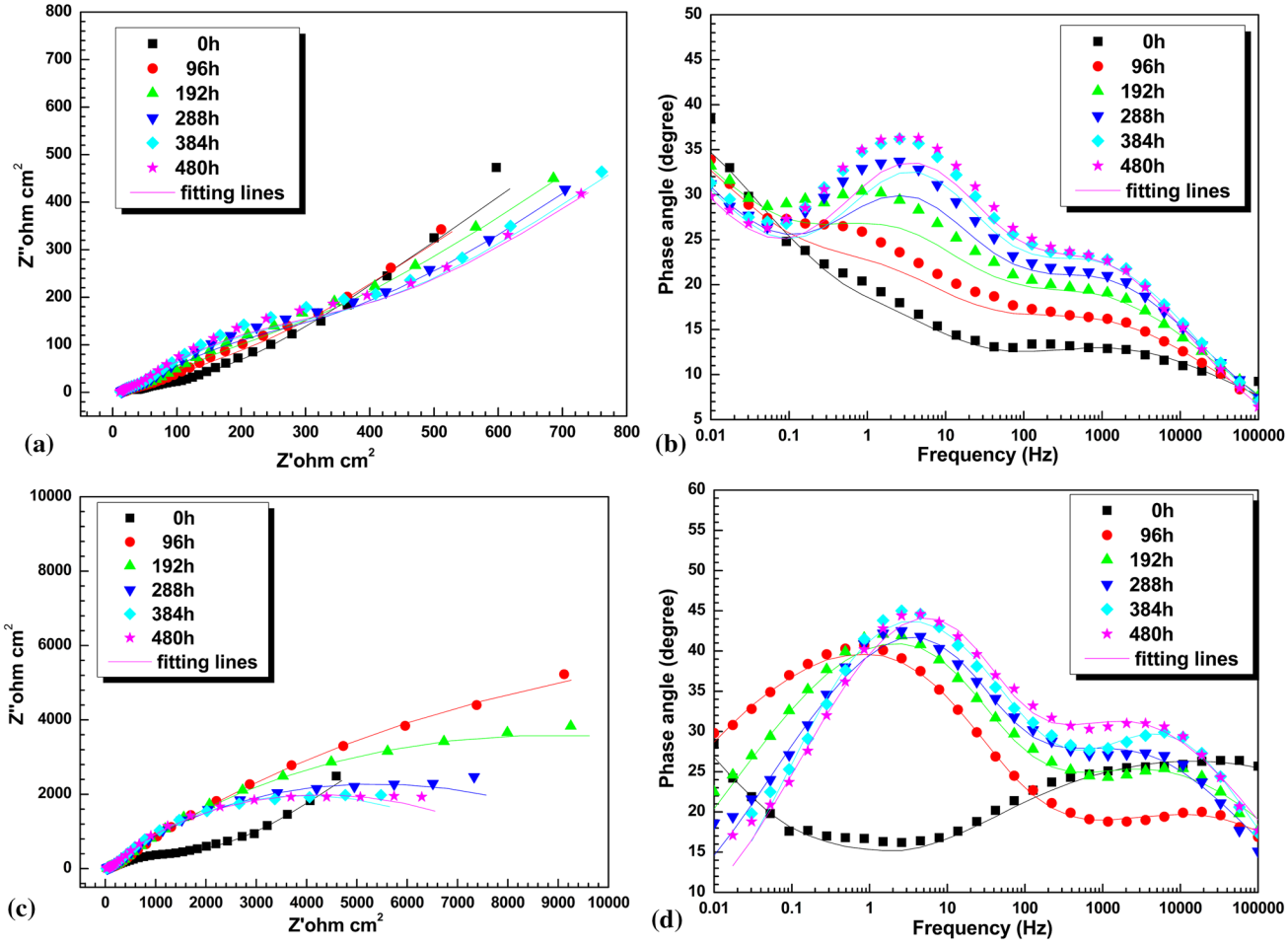

Fig. 1 Nyquist diagrams and Bode plots of copper under the two salt deposition conditions after different corrosion times: (a) and (b) for copper under the $MgCl_2$; (c) and (d) for copper under the NaCl

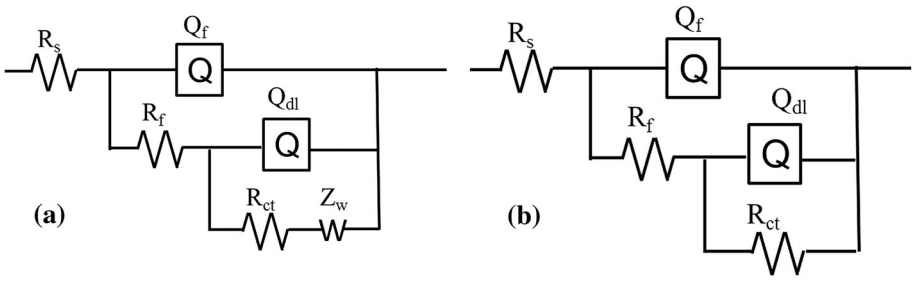

Fig. 2 Equivalent circuit models used to fit the experimental impedance data for copper: (a) for fitting the data displaying the Warburg impedance; (b) for fitting the data without displaying the Warburg impedance

two equivalent electrical circuits were employed to fit the in situ EIS data (Fig. 1). The first equivalent circuit was utilized to fit the EIS data containing the Warburg impedance, while the second circuit was used for the EIS data with only two capacitive loops. In Fig. 2, R_s is the solution resistance, Q_f and R_f represent the corrosion product film capacitance and resistance, respectively, Q_{dl} and R_{ct} represent the double electric layer and charge transfer resistances, respectively, and Z_w represents the Warburg impedance in the low-frequency region. Figure 1 shows that the fitting results are in good agreement with the experimental data in most of the frequency range, which indicates that the two equivalent circuits were suitable for the fitting of the in situ EIS data. The fitting parameters for copper under both deposition conditions are presented in Tables 1 and 2. It is known that if the impedance response exhibits more than one time constant, an erroneous corrosion rate is obtained in the calculation of R_p (Ref 23). Therefore, in this study, as the charge transfer resistance (R_{ct}) is more correlated to the corrosion rate, $1/R_{ct}$ can be used as an effective parameter to characterize the corrosion rates of copper exposed to both salt deposition conditions. Figure 3 shows the evolutions of $1/R_{ct}$ under both salt conditions as a function of the corrosion time. A distinct difference was observed between the values of $1/R_{ct}$. $1/R_{ct}$ of the copper under the $MgCl_2$ deposition

Table 1 The fitting results of EIS parameters of the copper under the $MgCl_2$ deposition condition

	0 h	96 h	192 h	288 h	384 h	480 h
R_s, Ω cm^2	29.54	16.79	14.13	11.72	10.8	9.955
Q_f, F cm^{-2} Hz^{1-nf}	6.88E−4	9.15E−4	7.05E−4	5.63E−4	4.67E−4	4.89E−4
n_f	0.3639	0.4012	0.4403	0.4815	0.5128	0.5245
R_f, Ω cm^2	115.3	81.81	78.25	66.16	63.7	54.08
Q_{dl}, F cm^{-2} Hz^{1-ndl}	1.59E−3	2.1E−3	1.33E−3	9.23E−4	6.93E−4	7.74E−4
n_{dl}	0.5858	0.5045	0.5355	0.6047	0.6432	0.6237
R_{ct}, Ω cm^2	179.8	337.3	451.3	408	419	445.7
Z_w	4.31E−3	5.08E−3	4.55E−3	6.03E−3	5.83E−3	6.45E−3

Table 2 The fitting results of EIS parameters of the copper under the NaCl deposition condition

	0 h	96 h	192 h	288 h	384 h	480 h
R_s, Ω cm^2	18.14	28.67	21.86	21.18	17.56	14.94
Q_f, F cm^{-2} Hz^{1-nf}	9.29E−5	1.39E−4	1.34E−4	1.46E−4	4.38E−5	1.20E−4
n_f	0.3419	0.3832	0.426	0.4537	0.573	0.4878
R_f, Ω cm^2	2716	311.7	414.1	454.1	172.1	408.4
Q_{dl}, F cm^{-2} Hz^{1-ndl}	3.62E−4	1.22E−4	6.45E−5	4.59E−5	1.24E−4	3.75E−5
n_{dl}	0.7851	0.5921	0.6552	0.7117	0.611	0.6501
R_{ct}, Ω·cm^2	1014	3.34E4	1.81E4	1.07E4	7651	8455
Z_w	9.37E−4	…	…	…	…	…

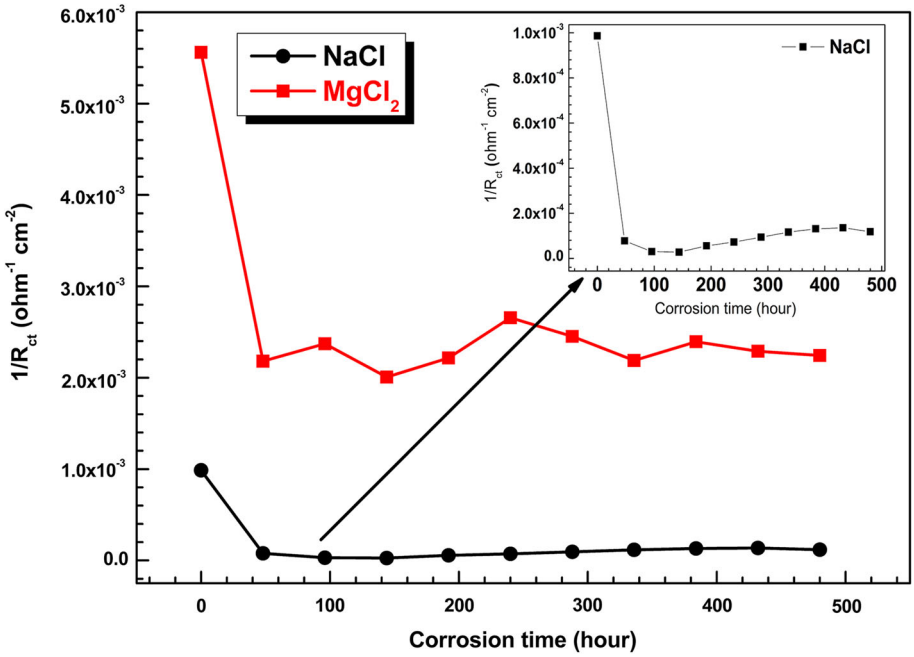

Fig. 3 Plot of the reciprocal of R_{ct} of copper under the $MgCl_2$ and NaCl salt deposition conditions as a function of corrosion time

condition was significantly higher than that for the NaCl deposition condition, indicating that the copper under the $MgCl_2$ deposition condition exhibited a more severe corrosion, which is consistent with the results of the weight loss measurement. In addition, fluctuations can be observed in the $1/R_{ct}$ plot of the copper under the $MgCl_2$ deposition condition, as the values of R_{ct} were very small and close to each other, indicating the low protectiveness of the corrosion products. $1/R_{ct}$ of the copper under the NaCl deposition condition initially decreased and then gradually increased, indicating that the structures and/or compositions of the corrosion product layer change, which may directly influence the corrosion rate of copper.

3.3 Morphologies of Corrosion Products

The corrosion product layer formed on the copper may influence the corrosion process owing to its diffusion barrier effect. Therefore, it is necessary to study the structures of the corrosion product layers formed during different corrosion periods. Figure 4 and 5 shows the surface morphologies of corrosion products formed on the samples during the whole corrosion process under both salt deposition conditions. Flaky corrosion products accumulated loosely on the tested sample in the case of the $MgCl_2$ deposition condition. However, the corrosion products formed on the copper under the NaCl deposition condition were more compact compared with those formed under the $MgCl_2$ deposition condition. More detailed information about the structures of the corrosion product layers can be obtained by observing their cross-sectional morphologies (Fig. 6 and 7). An apparent difference was observed between the structures of the corrosion product layers formed on copper under the two salt deposition conditions. Under the $MgCl_2$ deposition condition, the corrosion product was single-layered and extremely loose, leading to contamination of the epoxy resin with corrosion products during the embedding process (Fig. 6). Furthermore, no obvious change in the compactness of the corrosion products was observed with the progress of the corrosion. However, under the NaCl deposition condition, a double-layered corrosion product can be observed on the sample surface at all corrosion periods, consisting of inner and out layers, which were in contact with the substrate

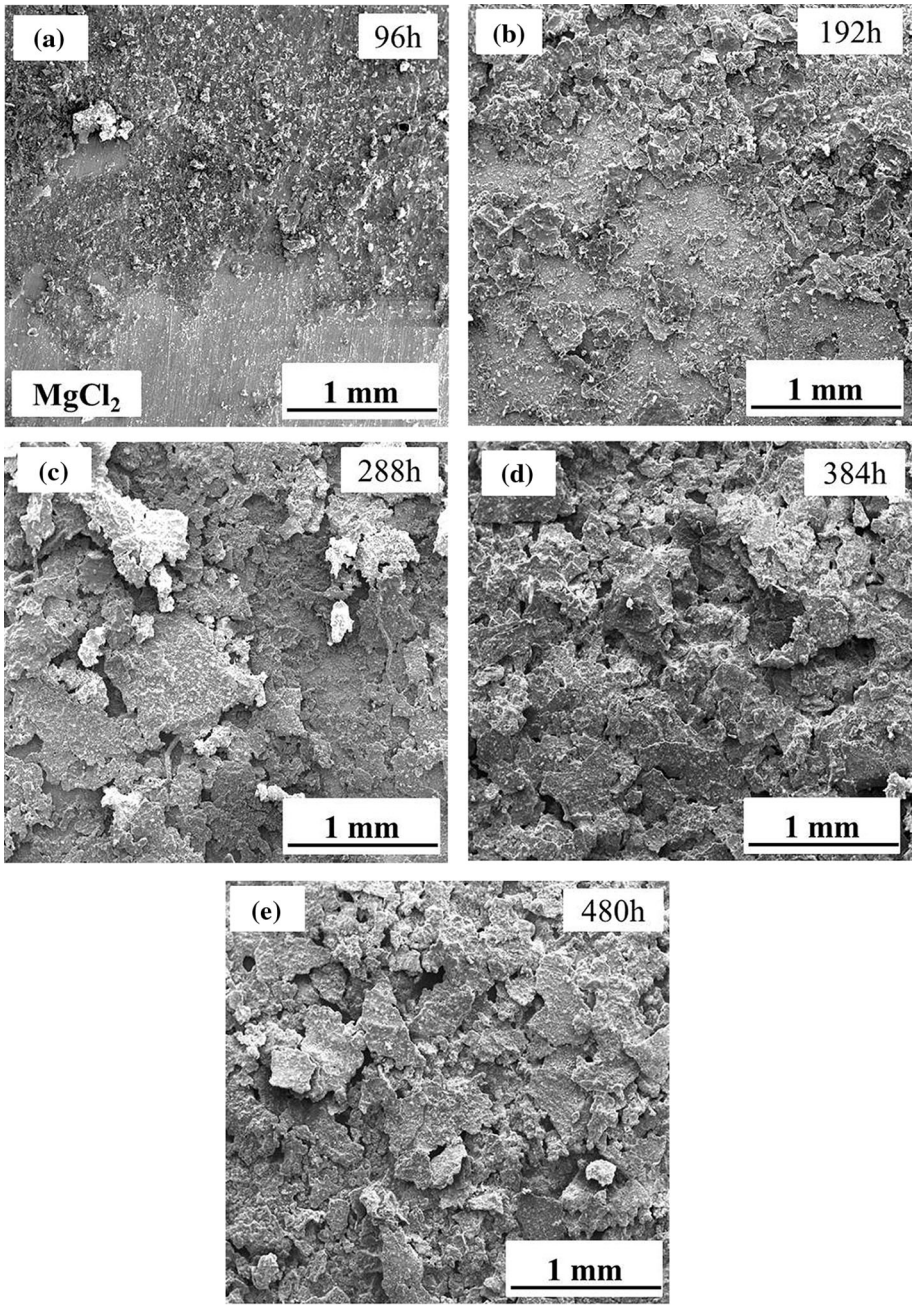

Fig. 4 Surface morphologies of corrosion products formed on the copper under the $MgCl_2$ salt deposition condition after different corrosion times

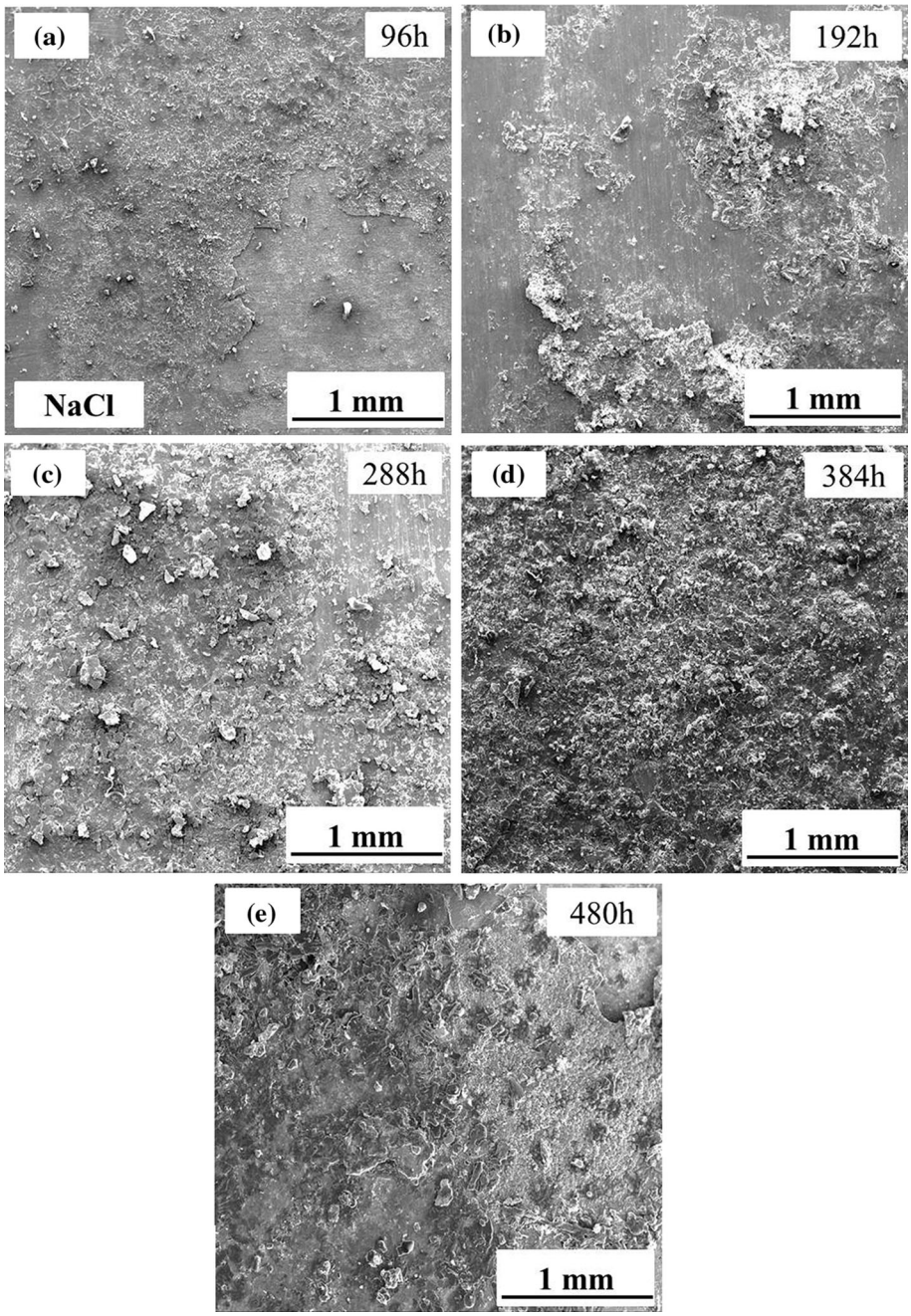

Fig. 5 Surface morphologies of corrosion products formed on the copper under the NaCl salt deposition condition after different corrosion times

and atmosphere, respectively (Fig. 7). In addition, with the progress of the corrosion, the compactness of the outer layer gradually decreased and then increased, which may be related to the changes in $1/R_{ct}$ of the copper under the NaCl deposition condition, as shown in Fig. 3.

3.4 Analysis of Corrosion Products

It has been shown that corrosion products are important in the whole corrosion process of metals (Ref 24). Therefore, the corrosion products formed on the copper under the $MgCl_2$ and NaCl salt deposition conditions were further analyzed by XRD. Figure 8 shows XRD patterns of the corrosion products formed on copper after different corrosion times under both salt deposition conditions. The composition of the corrosion products formed under the $MgCl_2$ deposition condition differs from that of the products formed under the NaCl deposition condition. In the case of the NaCl deposition condition, the main corrosion products formed on the copper were $Cu_2Cl(OH)_3$ and Cu_2O, while the corrosion products formed on the copper under the $MgCl_2$ deposition condition were composed of $Cu_2Cl(OH)_3$ and $Mg_2(OH)_3Cl{\cdot}4H_2O$, without Cu_2O. The presence of $MgCl_2$ may inhibit the formation of Cu_2O on the sample surface.

In order to further clarify the composition of the corrosion products formed on the copper, an elemental analysis was performed by EDS. Figure 9 presents SEM images showing the

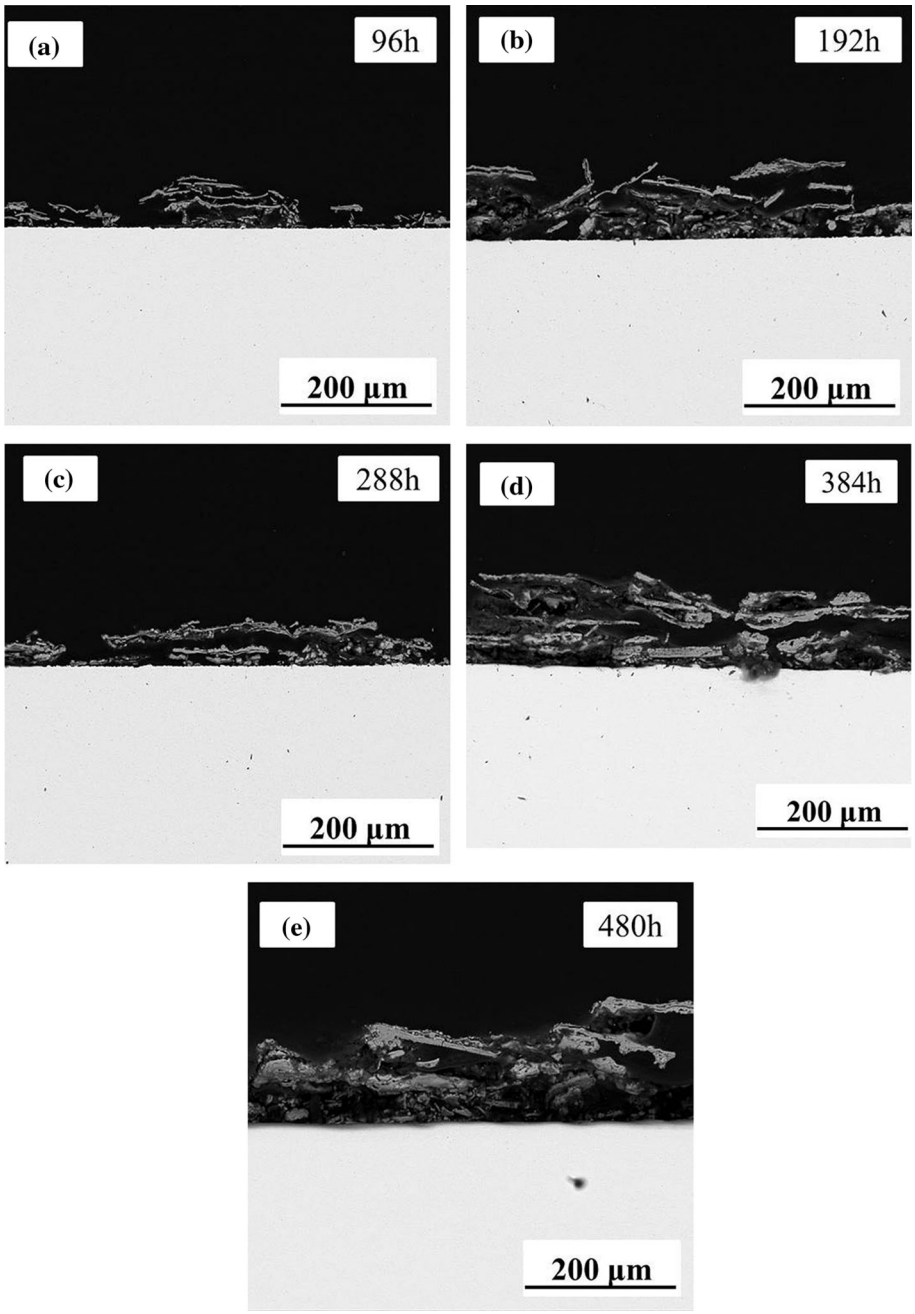

Fig. 6 Cross-sectional morphologies of corrosion products formed on the copper under the $MgCl_2$ salt deposition condition after different corrosion times

surface morphologies of the copper after removal of the loose outer layer corrosion products with a brush. EDS of corresponding sites is also shown in Fig. 9. The chemical compositions of the corresponding sites are presented in Table 3. Many small holes were uniformly distributed on the surface of the sample under the $MgCl_2$ deposition condition. The region outside the holes is composed only of Cu (spectrum A), while the region inside the holes contained not only Cu but also O, Cl, and Mg (spectrum B), indicating the formation of $Mg_2(OH)_3Cl{\cdot}4H_2O$. In the case of the NaCl deposition condition, an inner layer compact corrosion product can be observed on the copper, which is composed mainly of Cu and O and small amount of Cl (spectra C and D). XRD and SEM results show that the compact inner layer corrosion product consists of Cu_2O, while the loose outer layer consists of $Cu_2Cl(OH)_3$.

4. Discussion

4.1 Effect of the $MgCl_2$ Deposit on the Time of Wetness of Copper

The atmospheric corrosion of metals is significantly affected by the time of wetness, which depends on environmental factors including temperature, RH, and the presence of corrosive pollutants such as chlorides, which promote the

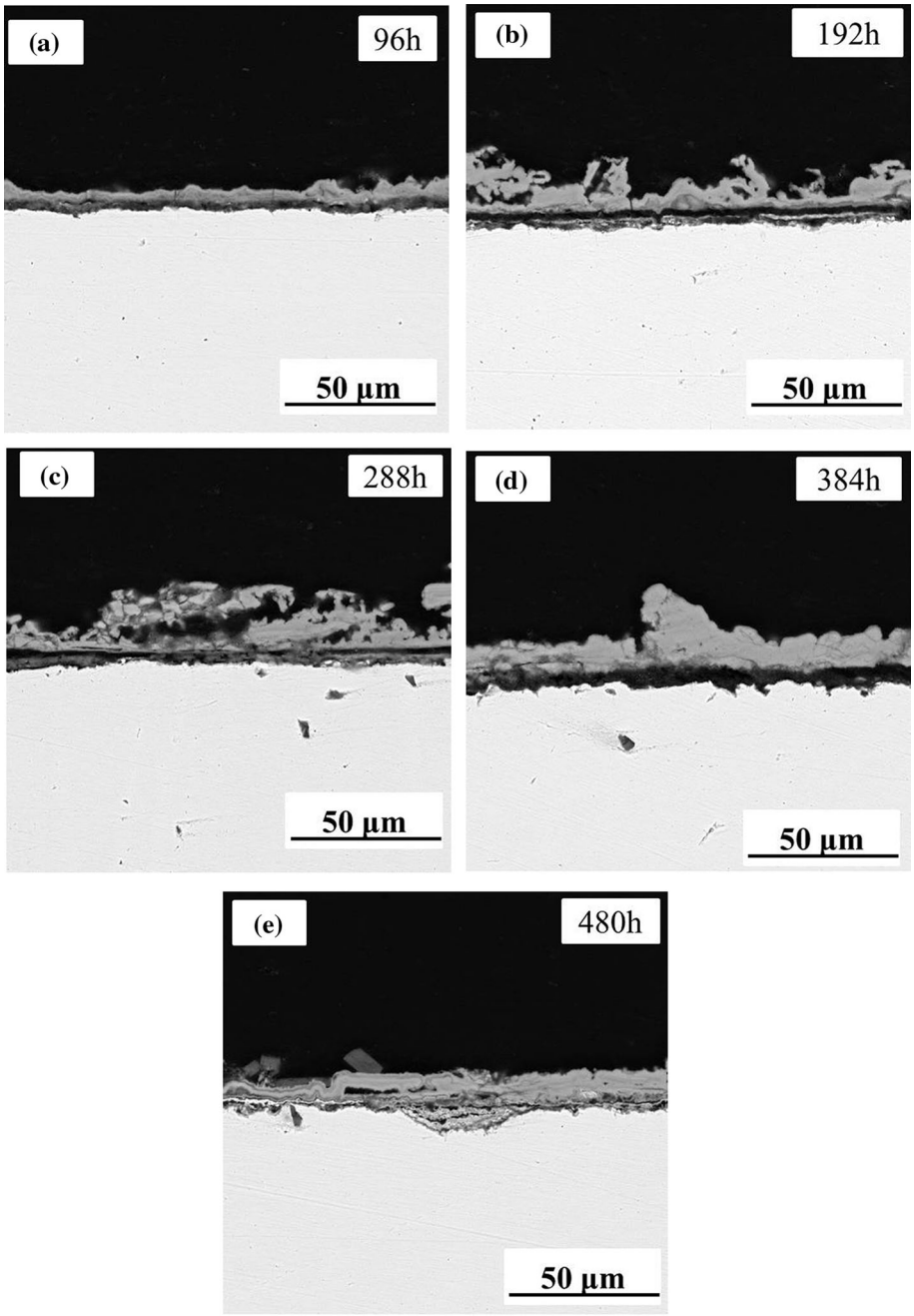

Fig. 7 Cross-sectional morphologies of corrosion products formed on the copper under the NaCl salt deposition condition after different corrosion times

corrosion of metals. It is known that the deliquescence relative humidity (DRH) of $MgCl_2$ (32%) is significantly lower than that of NaCl (75%), which implies that the time of wetness of copper under the $MgCl_2$ deposition condition was longer than that under NaCl during a wet/dry cycle. Therefore, compared to that under the NaCl deposition condition, the real corrosion time of copper under the $MgCl_2$ deposition condition was increased, which might lead to the severe corrosion of copper.

4.2 Effect of the $MgCl_2$ Deposit on the Corrosion Products of Copper

Electrochemical dissolution of copper occurs to form Cu^+ during the initial corrosion stage under thin electrolyte layers. Subsequently, Cu^+ is transformed into the insoluble CuCl and soluble $CuCl_2^-$ in the presence of Cl^-. $CuCl_2^-$ can be then converted to Cu_2O through precipitation or oxidized into $Cu_2(OH)_3Cl$ according to Eq (1) or (2), respectively (Ref 25, 26):

$$2CuCl_2^- + 2OH^- \leftrightarrow Cu_2O + H_2O + 4Cl^- \quad \text{(Eq 1)}$$

$$2CuCl_2^- + O_2 + 2H_2O \rightarrow 2Cu_2(OH)_3Cl(s) + OH^- \quad \text{(Eq 2)}$$

In this study, for the copper under the NaCl deposition condition, the main corrosion products Cu_2O and $Cu_2(OH)_3Cl$ formed gradually according to the above chemical reactions. However, the composition analysis of the corrosion products

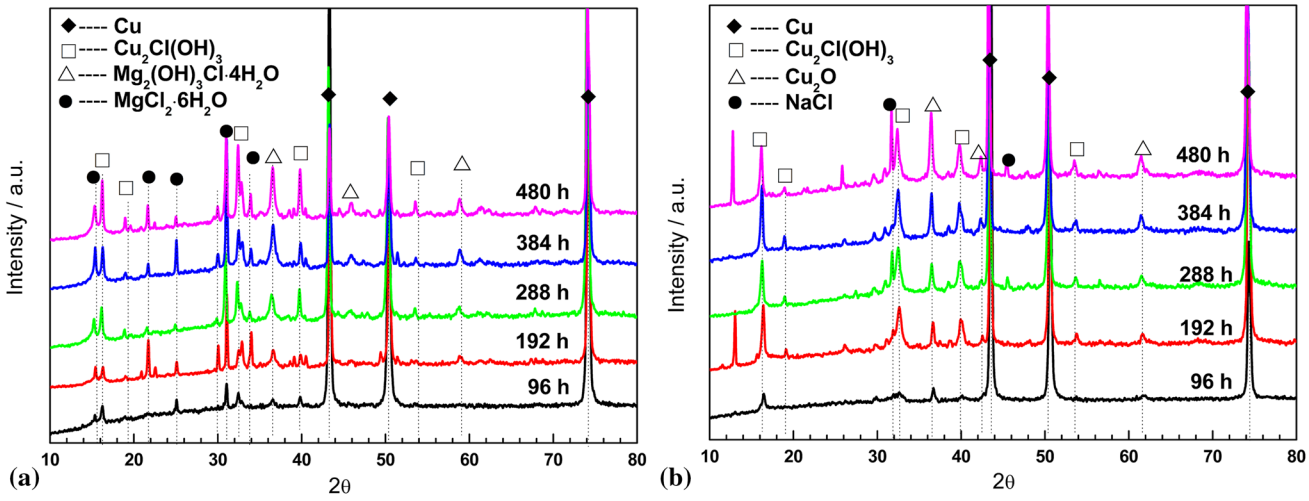

Fig. 8 XRD patterns of corrosion products formed on the copper under the $MgCl_2$ (a) and NaCl (b) salt deposition conditions for 96, 192, 288, 384, and 480 h

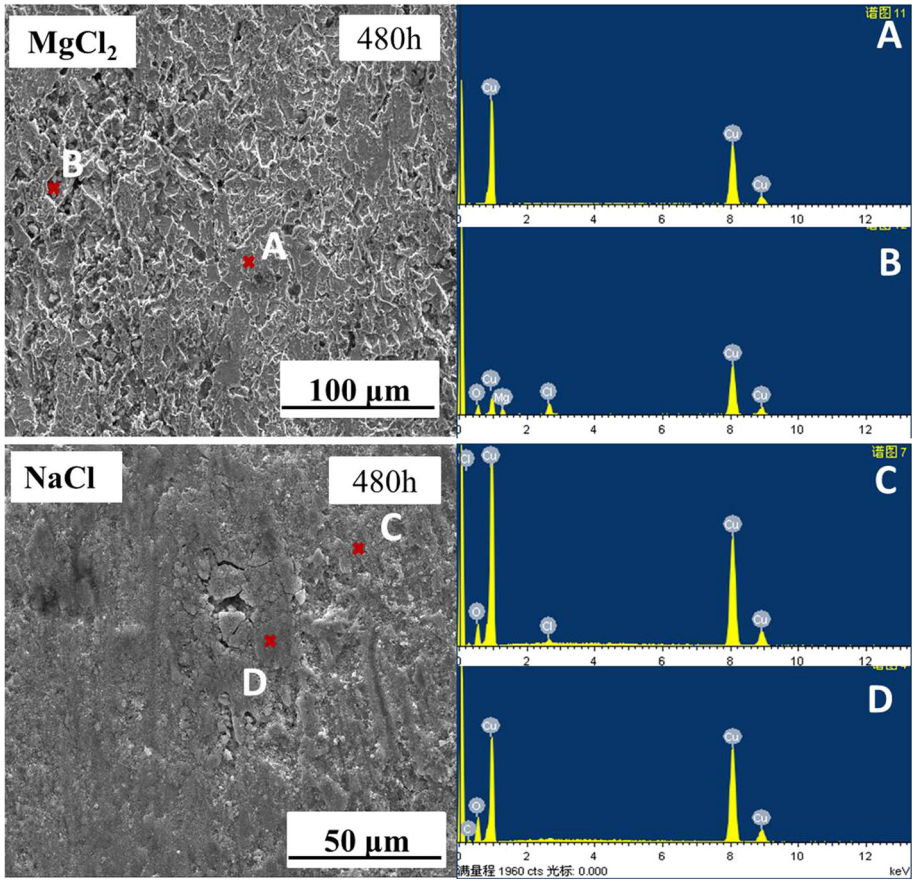

Fig. 9 SEM images and corresponding EDS spectra of corrosion products formed on the copper under the $MgCl_2$ and NaCl salt deposition conditions for 480 h

indicates that the formation of Cu_2O was suppressed under the $MgCl_2$ deposition condition. Cu_2O is a p-type semiconductor with a low electrical conductivity (Ref 27), which is mainly responsible for the protectiveness of copper. The lack of Cu_2O in the corrosion product layer implies that the corrosion rate of copper under the $MgCl_2$ salt deposition condition would increase. $MgCl_2$ restrains the formation of Cu_2O, as Mg^{2+} may react preferentially with OH^- and Cl^- to form $Mg_2(OH)_3Cl{\cdot}4H_2O$, which shifted the equilibriums in Eq (1) and (2) to left and right with the consumption of OH^-, respectively. Therefore, Cu_2O cannot be deposited in response to the left shift of Eq (1), and more $Cu_2(OH)_3Cl$ would be formed owing to the right shift of Eq (2), which is consistent with the composition analysis by XRD (Fig. 8). Therefore, the

absence of Cu_2O directly led to the severe corrosion of copper under the $MgCl_2$ deposition condition.

4.3 Effect of the $MgCl_2$ Deposit on the Corrosion Morphology of Copper

In order to further investigate the effect of the $MgCl_2$ deposit on the corrosion attack of copper, SEM was employed to observe the surface morphologies of copper after the removal of the corrosion products. Figure 10 presents a series of SEM images showing the surface morphologies of copper exposed for 480 h under both testing conditions after the removal of the corrosion products. The samples under the two deposition conditions have different corrosion morphologies. In the case of the $MgCl_2$ deposit, a uniform corrosion attack can be observed at a low magnification, as shown in Fig. 10a. However, when the surface was analyzed at a high magnification, many small corrosion pits can be observed on the sample surface (Fig. 10b). The region of one pit was further analyzed at a higher magnification (Fig. 10c). A similar intergranular corrosion occurred on the copper, which may lead to the formation of loosely packed corrosion products. In the case of the NaCl deposit, the local corrosion can be observed on the surface (Fig. 10d). A selected part from the corrosion region was observed at high magnifications (Fig. 10e and f). A uniform corrosion was observed on the copper under the NaCl deposition condition, which was significantly different from that under the $MgCl_2$ deposition condition. The loose corrosion products can lock water and promote the transport of oxygen to the metal surface, thus leading to the severe corrosion of the sample under the $MgCl_2$ deposition condition. On the contrary, the compact corrosion products formed on the copper under the NaCl deposition condition may act as a barrier to retard the diffusion of the corrosive electrolyte and oxygen, leading to a lower corrosion rate.

Table 3 The EDS results of the chemical composition of corresponding sites shown in Fig. 9

Element, wt.%	Cu	O	Cl	Mg
A	100	…	…	…
B	75.09	13.23	5.18	6.50
C	84.67	14.36	0.97	…
D	80.45	19.55	…	…

5. Conclusion

The atmospheric corrosion behaviors of copper under the $MgCl_2$ and NaCl deposition conditions were investigated. The experimental results showed that, compared to that under the NaCl deposition condition, the corrosion of copper under the $MgCl_2$ deposition condition was more severe. The main corrosion products formed on the tested sample in the case of the NaCl deposition condition consisted of $Cu_2Cl(OH)_3$ and Cu_2O, while those in the case of the $MgCl_2$ deposition condition consisted of $Cu_2Cl(OH)_3$ and $Mg_2(OH)_3Cl{\cdot}4H_2O$. Under the NaCl deposition condition, a double-layer structure formed during the corrosion, while the corrosion product layer formed on the copper under the $MgCl_2$ deposition condition had an extremely loose structure. $MgCl_2$ affected the corrosion of copper by inhibiting the formation of Cu_2O, which led to the severe corrosion.

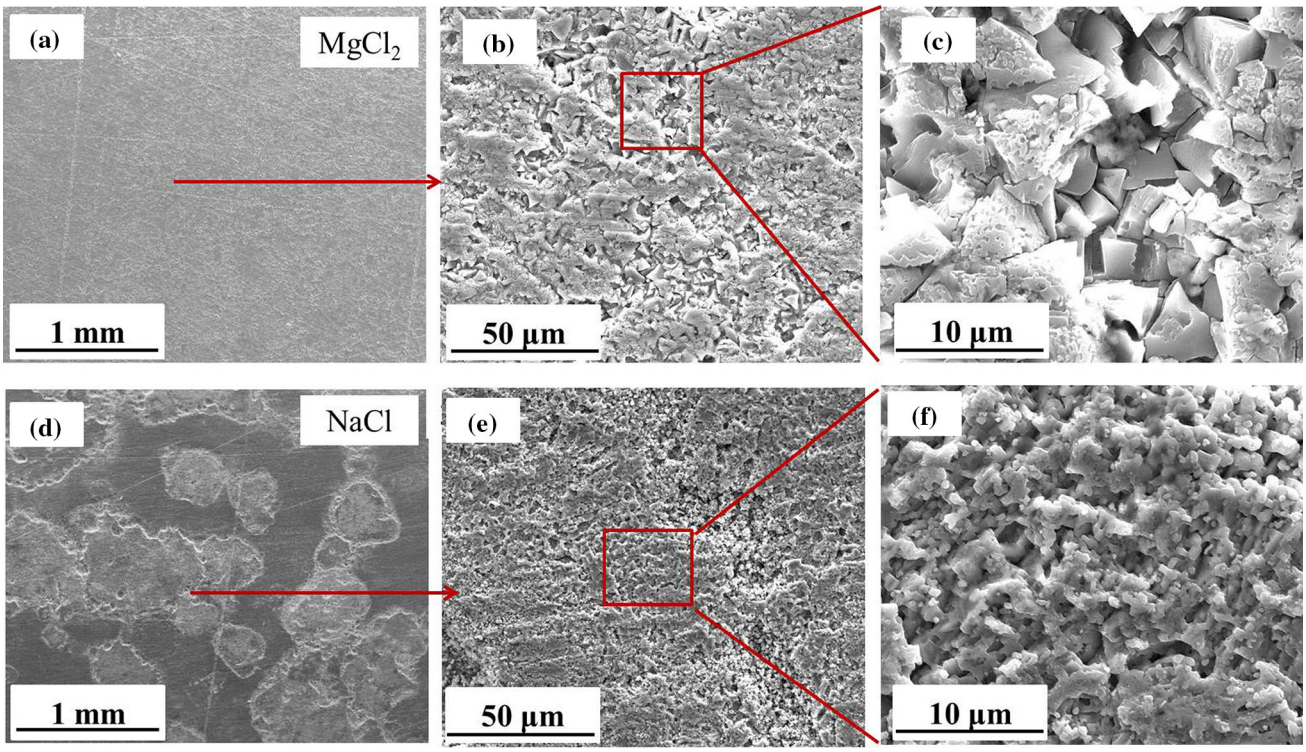

Fig. 10 Surface morphologies of the copper under the $MgCl_2$ (a)–(c) and NaCl (d)–(f) salt deposition conditions for 480 h after removing the corrosion products

Acknowledgments

The investigation is supported by the National Science Foundation of China (Nos. 51601199 and 51671197) and by the Guangzhou Industry-university-research Collaborative Innovation Alliance Special Project (201604046014).

References

1. Y.J. Liu, Study on Influence of Native Oxide and Corrosion Products on Atmospheric Corrosion of Pure Al, *Corros. Sci.*, 2014, **80**, p 169–176
2. W. Han, C. Pan, and Z.Y. Wang, A Study on the Initial Corrosion Behavior of Carbon Steel Exposed to Outdoor Wet/Dry Cyclic Condition, *Corros. Sci.*, 2014, **88**, p 89–100
3. Y.T. Ma, Y. Li, and F.H. Wang, The Atmospheric Corrosion Kinetics of Low Carbon Steel in a Tropical Marine Environment, *Corros. Sci.*, 2010, **52**, p 1796–1800
4. M.P. Zheng, Research and Prospection of the Whole World Salt Lake Geology, *Foreign Depos. Geol.*, 1989, **3**, p 1–34
5. Q.X. Li, Z.Y. Wang, W. Han, and E.H. Han, Characterization of the Rust Formed on Weathering Steel Exposed to Qinghai Salt Lake Atmosphere, *Corros. Sci.*, 2008, **50**, p 365–371
6. J. Wang, Z.Y. Wang, and W. Ke, Corrosion Behavior of Weathering Steel in Diluted Qinghai Salt Lake Water in a Laboratory Accelerated Test that Involved Cyclic Wet/Dry Conditions, *Mater. Chem. Phys.*, 2010, **124**, p 952–958
7. J. Wang, Z.Y. Wang, and W. Ke, Characterisation of Rust Formed on Carbon Steel after Exposure to Open Atmosphere in Qinghai Salt Lake Region, *Corros. Eng. Sci. Technol.*, 2012, **47**, p 125–130
8. B.B. Wang, Z.Y. Wang, W. Han, and W. Ke, Atmospheric Corrosion of Aluminium Alloy 2024–T3 Exposed to Salt Lake Environment in Western China, *Corros. Sci.*, 2012, **59**, p 63–70
9. A.R. Mendoza, F. Corvo, A. Gomez, and J. Gomez, Influence of the Corrosion Products of Copper on Its Atmospheric Corrosion Kinetics in Tropical Climate, *Corros. Sci.*, 2004, **46**, p 1189–1200
10. J. Wu, X.G. Li, C.F. Dong, S.P. Zhang, and J.L. Zhou, Initial Corrosion Behavior of Copper and Brass in Tropical Maritime Atmospheric Environment, *J. Chin. Soc. Corros. Prot.*, 2012, **32**, p 70–79
11. I.T.E. Fonseca, R. Picciochi, M.H. Medonca, and A.C. Ramos, The Atmospheric Corrosion of Copper at Two Sites in Portugal: A Comparative Study, *Corros. Sci.*, 2004, **46**, p 547–561
12. H.L. Huang, Z.Q. Pan, X.P. Guo, and Y.B. Qiu, Effect of an Alternating Electric Field on the Atmospheric Corrosion Behavior of Copper Under a Thin Electrolyte Layer, *Corros. Sci.*, 2013, **75**, p 100–105
13. Ch Kleber, U. Hilfrich, and M. Schreiner, In Situ QCM and TM–AFM Investigations of the Early Stages of Degradation of Silver and Copper Surfaces, *Appl. Surf. Sci.*, 2007, **253**, p 3712–3721
14. X.Y. Zhang, W.L. He, I.O. Wallinder, J.S. Pan, and C. Leygraf, Determination of Instantaneous Corrosion Rates and Runoff Rates of Copper from Naturally Patinated Copper During Continuous Rain Events, *Corros. Sci.*, 2002, **44**, p 2131–2151
15. C. Pan, W.Y. Lv, Z.Y. Wang, W. Su, C. Wang, and S.N. Liu, Atmospheric Corrosion of Copper Exposed in a Simulated Coastal–Industrial Atmosphere, *J. Mater. Sci. Tech.*, 2017, **33**, p 587–595
16. ISO 8407, *Corrosion of Metal and Alloys–Removal of Corrosion Products from Corrosion Test Specimens*, The International Organization for Standardization (ISO), Geneva, 2009
17. W.J. Lorenz and F. Mansfeld, Determination of Corrosion Rates by Electrochemical DC and AC Methods, *Corros. Sci.*, 1981, **21**, p 647–672
18. C.L. Li, Y.T. Ma, Y. Li, and F.H. Wang, EIS Monitoring Study of Atmospheric Corrosion Under Variable Relative Humidity, *Corros. Sci.*, 2010, **52**, p 3677–3686
19. C. Thee, L. Hao, J.H. Dong, X. Mu, X. Wei, X.F. Li, and W. Ke, Atmospheric Corrosion Monitoring of a Weathering Steel Under an Electrolyte Film in Cyclic Wet/Dry Condition, *Corros. Sci.*, 2014, **78**, p 130–137
20. S.X. Li, J.H. Dong, E.H. Han, and W. Ke, Evolvement of Electrochemical Impedance Spectra of a Bi–electrode Cell for Carbon Steel in the Initial Stage of Wet/Dry Process, *Corros. Sci. Prot. Technol.*, 2007, **19**, p 167–170
21. Y. Van Ingelgem, E. Tourwé, J. Vereecken, and A. Hubin, Application of Multisine Impedance Spectroscopy, FE–AES and FE–SEM to Study the Early Stages of Copper Corrosion, *Electrochim. Acta*, 2008, **53**, p 7523–7530
22. G. Žerjav and I. Milošev, Protection of Copper Against Corrosion in Simulated Urban Rain by the Combined Action of Benzotriazole, 2–Mercaptobenzimidazole and Stearic Acid, *Corros. Sci.*, 2015, **98**, p 180–191
23. Y.L. Cheng, Z. Zhang, F.H. Cao, J.F. Li, J.Q. Zhang, J.M. Wang, and C.N. Cao, A Study of the Corrosion of Aluminum Alloy 2024–T3 Under Thin Electrolyte Layers, *Corros. Sci.*, 2004, **46**, p 1649–1667
24. M. Yamashita, H. Konishi, and T. Kozakura, In Situ Observation of Initial Rust Formation Process on Carbon STEEL under Na_2SO_4 and NaCl Solution Film with Wet/Dry Cycles Using Synchrotron Radiation x–rays, *Corros. Sci.*, 2005, **47**, p 2492–2498
25. G. Faita, G. Fiori, and D. Salvadore, Copper Behavior in Acid and Alkaline Brines–I, Kinetics of Anodic Dissolution in 0.5 M NaCl and Free–Corrosion Rates in the Presence of Oxygen, *Corros. Sci.*, 1975, **15**, p 383–392
26. X.N. Liao, F.H. Cao, L.Y. Zheng, W.J. Liu, A.N. Chen, J.Q. Zhang, and C.N. Cao, Corrosion Behavior of Copper Under Chloride–Containing Thin Electrolyte Layer, *Corros. Sci.*, 2011, **53**, p 3289–3298
27. P. Druska, H.H. Strehblow, and S. Golledge, A Surface Analytical Examination of Passive Layers on CuNi Alloys: PartI. Alkaline solution, *Corros. Sci.*, 1996, **38**, p 835–851